



# A New “Geometric” Mapping Function for the Hydrostatic Delay at GPS Frequencies

U. Foelsche and G. Kirchengast

Institute for Geophysics, Astrophysics and Meteorology, University of Graz, Universitaetsplatz 5, A-8010 Graz, Austria

Received 26 July 2000; accepted 24 October 2000

**Abstract.** The hydrostatic mapping function,  $m(\epsilon)$ , is a dimensionless factor which describes the elevation angle dependence of the hydrostatic path delay and relates the line of sight delay to the zenith delay. We have developed a simple “geometric” mapping function where the only free parameter (besides the elevation angle,  $\epsilon$ ) is the climatological pressure scale height. The value of  $m(\epsilon)$  is given by the ratio of the straight-line ray path length within the first two scale heights above the surface and the “effective height” defined by these first two scale heights. We used simulated neutral delays at GPS frequencies derived from high resolution ECMWF (European Centre for Medium-Range Weather Forecasts) atmospheric analysis fields (T213L50, T213L60) at different latitudes to compare the new mapping function with others currently in use (we compare with the Niell and the Davis mapping function, respectively, most frequently encountered in literature).

At elevations  $> 6^\circ$  the geometric mapping function displays, without involving any meteorological data, comparable or better accuracy and precision than the other mapping functions. © 2001 Elsevier Science Ltd. All rights reserved

## 1 Introduction

For a plane parallel model of the Earth and the atmosphere (neglecting the curvature of the Earth and azimuthal variations within the atmosphere), the hydrostatic delay in an arbitrary slant direction,  $\Delta L_h$  is given by the simple cosecant law

$$\Delta L_h = \frac{1}{\sin(\epsilon)} \Delta L_h^0 = \csc(\epsilon) \Delta L_h^0, \quad (1)$$

where  $\epsilon$  is the elevation angle of the radio source and  $\Delta L_h^0$  is the zenith hydrostatic delay. In general,  $\Delta L_h$  can be written as

$$\Delta L_h = m(\epsilon, \mathbf{p}) \Delta L_h^0. \quad (2)$$

The function  $m(\epsilon, \mathbf{p})$  depends on the elevation angle  $\epsilon$  and on the vector  $\mathbf{p}$ , which is some parameterized representation of the refractivity in the atmosphere (Davis et al., 1985), usually called *mapping function*. By convention, the dependence on the vector  $\mathbf{p}$  is commonly suppressed for the sake of simplicity of notation. Potential azimuthal dependence of the function is neglected in this formulation.

## 2 The “geometric” mapping function

We have developed a simple mapping function, where the only free parameter is the climatological pressure scale height. The value of  $m(\epsilon)$  is given by the ratio of the slant straight-line ray path length,  $S_{atm}$  within an “effective height” of the atmosphere,  $H_{atm}$ , defined by the first two scale heights above the surface, and  $H_{atm}$  itself

$$m(\epsilon) = \frac{S_{atm}}{H_{atm}}. \quad (3)$$

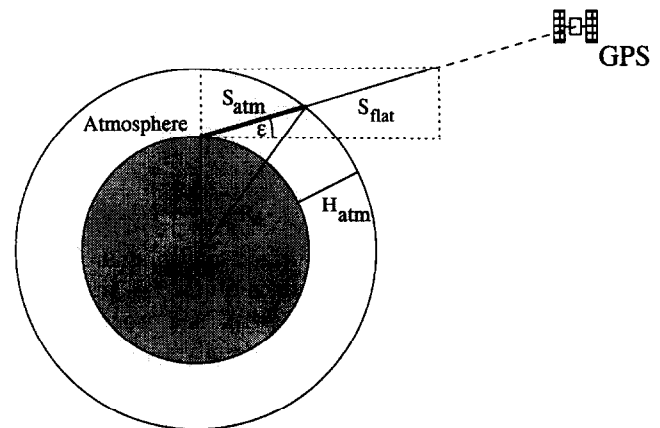


**Fig. 1.** Schematic illustration of the “geometric” mapping function.  $R_e$  is the radius of the Earth,  $\epsilon$  is the elevation angle of the GPS satellite, the “effective height” of the atmosphere,  $H_{atm}$ , is defined in the text.  $S_{atm}$  is the straight line ray path within  $H_{atm}$ , and  $S_{flat}$  is the corresponding ray path in a flat (plane-parallel) atmosphere.

Equation (3) can alternatively be written as:

$$m(\varepsilon) = \frac{1}{\sin(\varepsilon) \frac{S_{flat}}{S_{atm}}}, \quad (4)$$

in order to directly express the deviation from the simple cosecant law. In a plane-parallel atmosphere (i.e., for sufficiently high elevation angles), the "geometric" mapping function degenerates to the cosecant law.  $S_{atm}$  can be readily determined by evaluation of the triangle formed by  $R_e$ ,  $R_e + H_{atm}$ , and  $S_{atm}$  (see Fig. 1), where  $R_e$  is the radius of the earth. In general, it is sufficient to use a mean climatological scale height value of 7.5 km, yielding  $H_{atm} = 15.0$  km, as a globally applied constant.

Introducing the dimensionless ratio

$$\tilde{r} = \frac{R_e}{R_e + H_{atm}}, \quad (5)$$

the path length within the effective height,  $H_{atm}$ , can be expressed as:

$$S_{atm} = (R_e + H_{atm}) [\cos(\arcsin(\tilde{r} \cos \varepsilon)) - \tilde{r} \sin \varepsilon], \quad (6)$$

and Eq. (3), the "geometric" mapping function, can be written explicitly as

$$m(\varepsilon) = \left( \frac{R_e}{H_{atm}} + 1 \right) [\cos(\arcsin(\tilde{r} \cos \varepsilon)) - \tilde{r} \sin \varepsilon]. \quad (7)$$

### 3 Davis and Niell mapping function

The new mapping function was compared with the Davis and the Niell mapping functions, which are often used and frequently encountered in literature.

The *Davis mapping function* (Davis et al., 1985) is a modification of the continued fraction expansion introduced by Marini (1972)

$$m(\varepsilon) = \frac{1}{\sin \varepsilon + \frac{a}{\tan \varepsilon + \frac{b}{\sin \varepsilon + c}}}, \quad (8)$$

where  $c$  is a constant (-0.0090) and  $a$  and  $b$  are functions of surface temperature  $T_0$  in [°C], surface total pressure  $p_0$  in [hPa], water vapor partial pressure at surface  $e_0$  in [hPa], height of the troposphere  $h_T$  in [km], and tropospheric temperature lapse rate  $\beta$  in [K/km], respectively, with

$$\begin{aligned} a &= 0.001185 [1 + 0.6071 \cdot 10^{-4} (p_0 - 1000) \\ &- 0.1471 \cdot 10^{-3} e_0 + 0.3072 \cdot 10^{-2} (T_0 - 20) \\ &+ 0.1965 \cdot 10^{-1} (\beta + 6.5) - 0.5645 \cdot 10^{-2} (h_T - 11.231)] \end{aligned} \quad (9)$$

and

$$\begin{aligned} b &= 0.001144 [1 + 0.1164 \cdot 10^{-4} (p_0 - 1000) \\ &+ 0.2795 \cdot 10^{-3} e_0 + 0.3109 \cdot 10^{-2} (T_0 - 20) \\ &+ 0.3038 \cdot 10^{-1} (\beta + 6.5) - 0.1217 \cdot 10^{-1} (h_T - 11.231)]. \end{aligned} \quad (10)$$

The *Niell mapping function* (Niell, 1996) adopts a similar form, but does not depend on meteorology data

$$m(\varepsilon) = \frac{1 + \frac{a}{1 + \frac{b}{1 + c}}}{\sin \varepsilon + \frac{a}{\sin \varepsilon + \frac{b}{\sin \varepsilon + c}}}. \quad (11)$$

At each latitude the coefficients  $a$ ,  $b$ , and  $c$  are modeled as sinusoids in time, the phase is defined by doy = 28, corresponding to the winter extremum, e.g.,

$$a(\varphi, \text{doy}) = a_{avg}(\varphi) - a_{ampl}(\varphi) \cos\left(2\pi \frac{\text{doy} - 28}{365.25}\right). \quad (12)$$

### 4 Comparison - method

High resolution (T213) analysis fields from the European Centre for Medium-Range Weather Forecasts (ECMWF) for September 15, 1999, 12UT (L50) and January 15, 2000, 12UT (L60), respectively, were used to derive simulated slant hydrostatic delays. We performed high-precision 3D ray tracing of slant rays for elevation angles between 5° and 15° (south-looking, 1° steps in the meridional plane) and geographic latitudes between 0°N and 80°N (10° spacing), at meridians 0°E, 90°W, and 180°W, respectively. The slant hydrostatic delay was calculated as

$$\begin{aligned} \Delta L_h &= 10^{-6} \int_S N_{\text{hyd}}(s) ds + \Delta L_g = \\ &= \frac{k_1}{10^6} \frac{R^*}{m_d} \int_S \rho(s) ds + \Delta L_g, \end{aligned} \quad (13)$$

where  $N_{\text{hyd}}$  is the hydrostatic component of the refractivity  $N$ ,  $\Delta L_g$  is the "geometric delay" (the difference between the curved ray path  $S$  and the straight-line transmitter-receiver distance),  $k_1 = 77.60$  K/hPa,  $R^*$  is the universal gas constant (8314.51 Jkmol<sup>-1</sup>K<sup>-1</sup>),  $\rho$  is the total air density, and  $m_d$  is the molar mass of dry air (28.9644 kg/kmol). A minor error is introduced as the bended ray path  $S$  is determined by the  $N_{\text{hyd}}$ -field and not by the complete  $N$ -field of the atmosphere.

In zenith direction (indicated by the superscript "0") the geometric delay vanishes and the hydrostatic delay can be estimated given the total surface pressure  $p_0$

$$\Delta L_n^0 = \frac{k_1 R^*}{10^6 m_d} \int_0^\infty \rho(z) dz \equiv \frac{k_1 R^*}{10^6 m_d g_m} \frac{p_0}{f(\varphi, H)}, \quad (14)$$

with  $g_m = 9.7837 \text{ m/s}^2$ , and

$$f(\varphi, H) = 1 - 0.00265 \cos 2\varphi - 0.000285H, \quad (15)$$

where  $\varphi$  is the geographic latitude and  $H$  is the station height in [km] (Saastamoinen, 1972; Elgered, 1993).

Zenith hydrostatic delays for each synthetic ground station were modeled using Eq. (14) and mapped onto the different ray paths using the three mapping functions described above. The results were compared with the simulated slant hydrostatic delays obtained by the high-precision ray tracing.

### 5 Comparison - results

In a first step we compared modeled and simulated ("measured") delays at high elevations to check the performance of the ray tracer and the match of Eq. (14) delays with realistically simulated delays through ECMWF analysis fields. Simulated slant hydrostatic delays at  $89^\circ$  elevation in opposite directions display a maximum difference of only 0.05 mm, confirming that ray tracer errors are negligible.

The differences between simulated and modeled zenith hydrostatic delays show a very similar latitude-dependence for every meridian considered, with minimum values at mid latitudes (see Fig. (2) below).

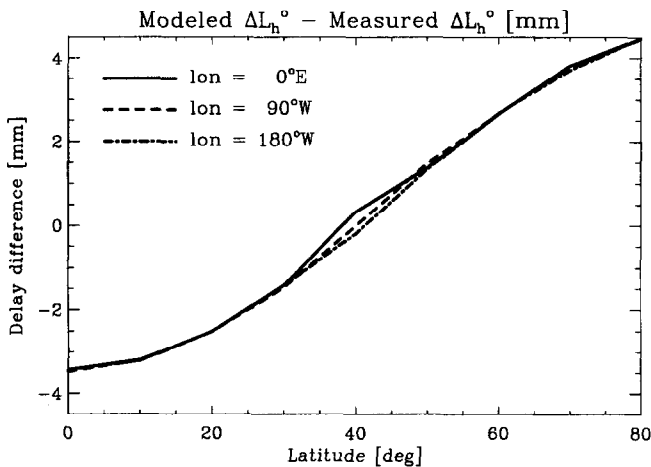


Fig. 2. Difference between modeled (Eq. (14)) and "measured" (realistically simulated) zenith hydrostatic delays for three meridionally oriented chains of synthetic receivers with  $10^\circ$  latitude spacing.

Currently we are not able to explain this latitude-dependent difference. However, given that one would not expect  $>2$  mm differences if hydrostatic equilibrium is valid

in the ECMWF analysis fields used, this is an interesting result deserving further inquiry and explanation.

Coefficients for the Niell mapping function were modeled as indicated above (see Niell, 1996, for details), coefficients for the Davis mapping function were computed with "true" meteorological values (a most favorable choice, as "true" ones never will be available in practice).

The general behavior of the different mapping functions at  $90^\circ\text{W}$  for September 15, 1999 can be examined in Fig. (3) above. A more quantitative representation was chosen for  $0^\circ\text{E}$  and  $180^\circ\text{W}$  (Fig. (4) and Fig. (5), respectively).

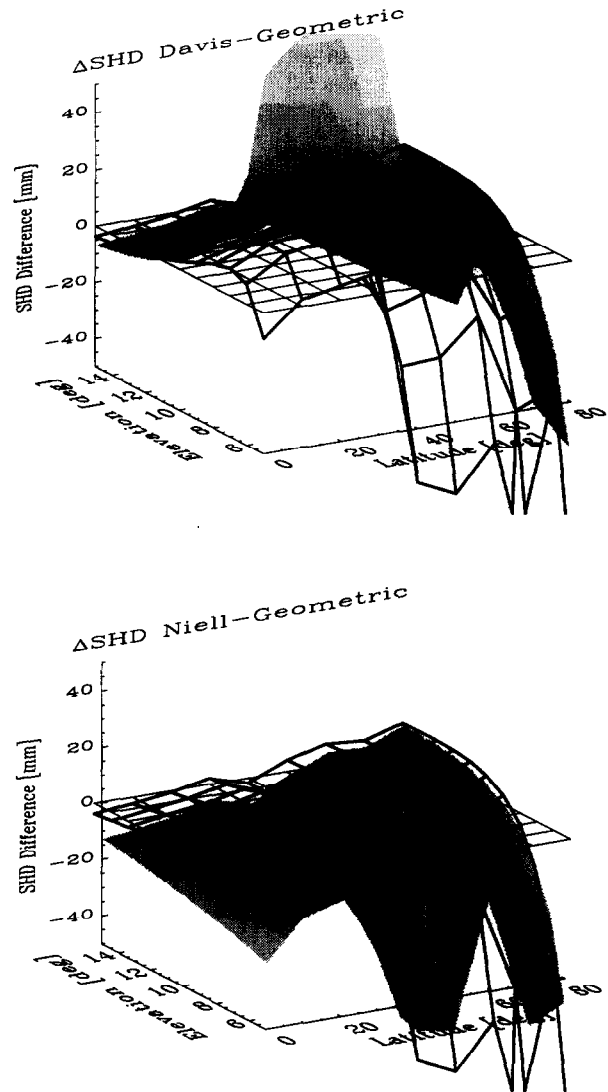
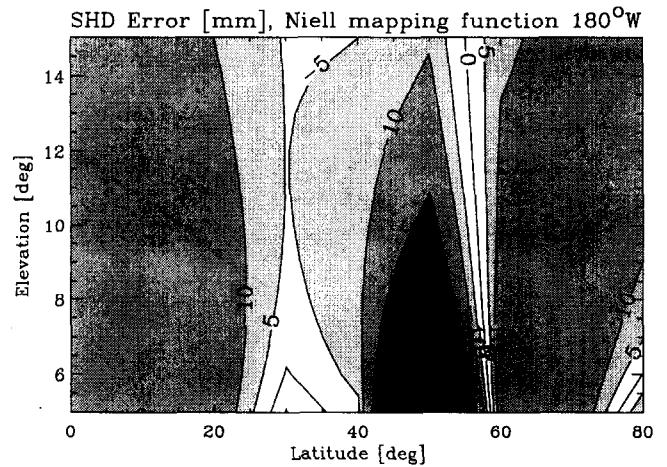
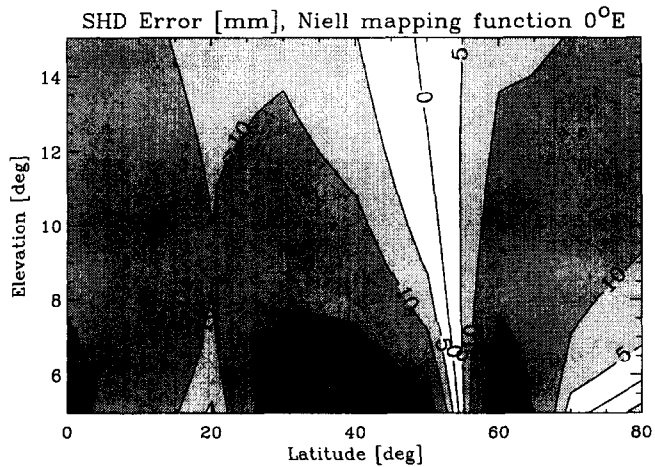
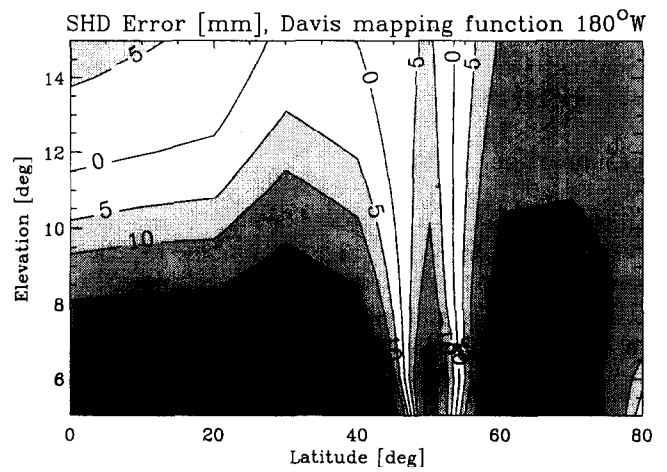
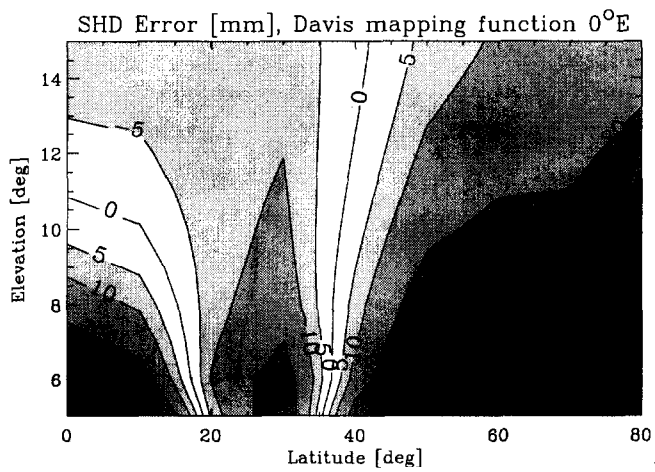
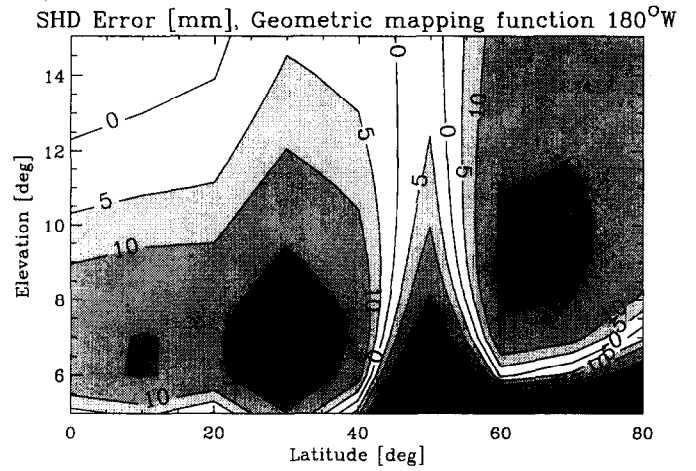
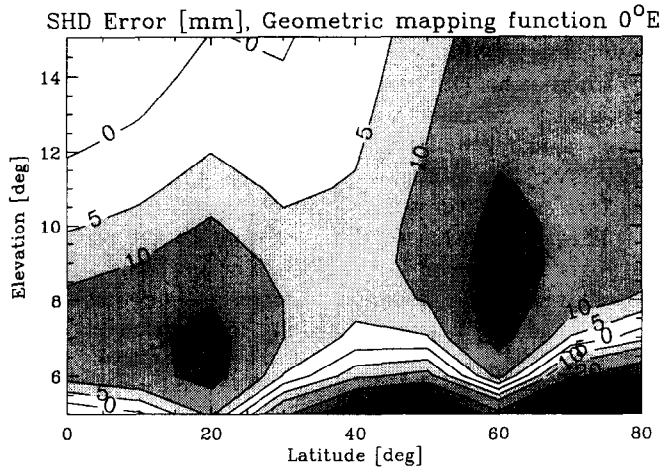


Fig. 3. Differences between modeled and "measured" slant hydrostatic delays for September 15, 1999, 12UT at  $90^\circ\text{W}$ . Top panel: geometric (surface grid) and Davis mapping function (shaded), bottom panel: geometric (surface grid) and Niell mapping function (shaded).

At elevations  $< 6^\circ$  the geometric mapping functions shows a sudden decrease in performance but above this elevation, the results are comparable to or better than when using the other two mapping functions.



**Fig. 4.** Differences between modeled and "measured" slant hydrostatic delays for September 15, 1999, 12UT at  $0^{\circ}\text{E}$  using the geometric (top panel), the Davis (middle panel), and the Niell mapping function (bottom panel), respectively.

**Fig. 5.** Differences between modeled and "measured" slant hydrostatic delays for September 15, 1999, 12UT, at  $180^{\circ}\text{W}$  longitude using the geometric (top panel), the Davis (middle panel), and the Niell mapping function (bottom panel), respectively.

In order to investigate seasonal variations we performed an equivalent analysis with ECMWF T213L60 fields for January 15, 2000, 12 UT. An example for 180°W is shown in Fig. (6).

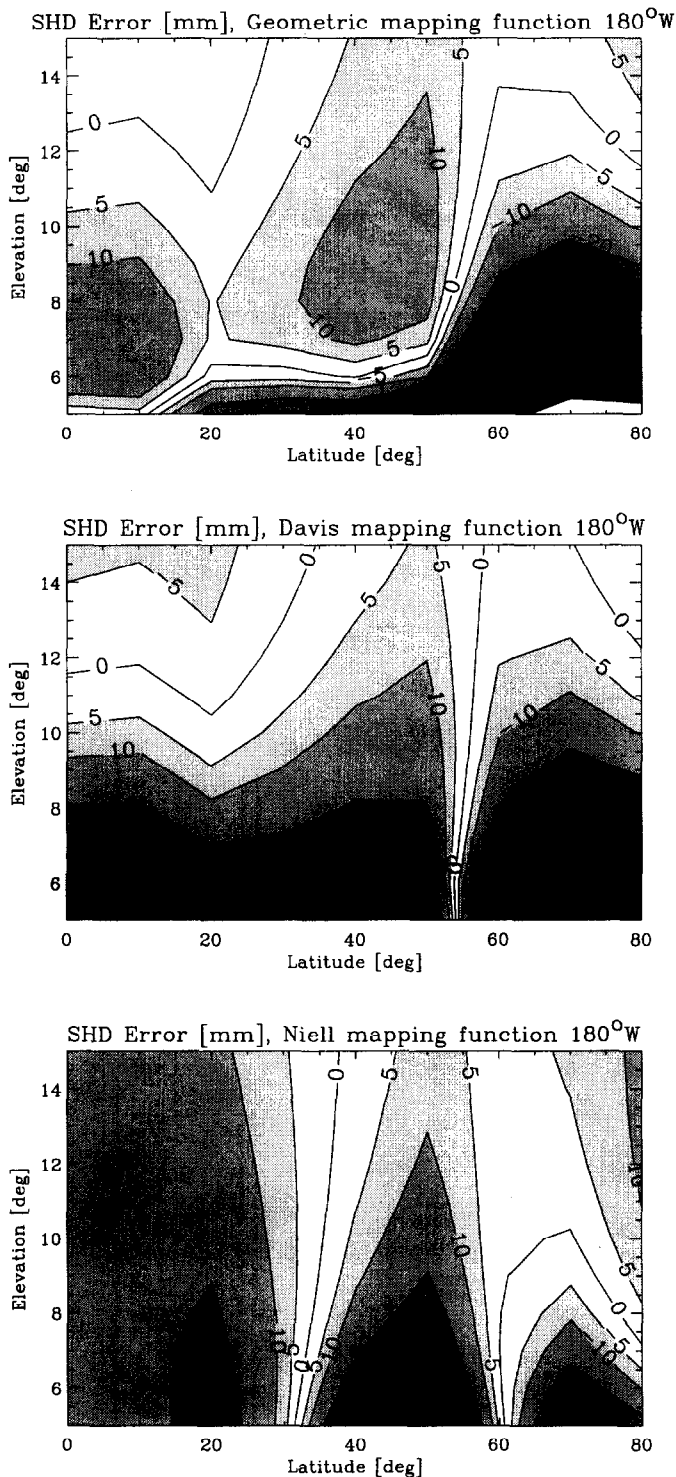


Fig. 6. Differences between modeled and "measured" slant hydrostatic delays for January 15, 2000, 12UT, at 180°W longitude using the geometric (top panel), the Davis (middle panel), and the Niell mapping function (bottom panel), respectively.

For the effective height,  $H_{\text{atm}}$ , in the geometric mapping function we used exactly the same value (15.0 km) as in the September case.

Besides a small domain at high latitudes and low elevations angles, the geometric mapping function again displays a good performance with slant hydrostatic delay differences of < 10 mm in the major part of the domain.

To put the result into perspective, it should be noticed that the slant hydrostatic delay reaches typical values of ~23 m at 5° elevation.

## 6 Summary and conclusions

We have presented a new simple mapping function based on geometrical considerations, which does not depend on meteorological data. The only free parameter is an "effective height" of the atmosphere defined by the first two pressure scale heights for which it is generally sufficient to use a global mean constant value.

At least in a fairly realistic "simulated world" (ECMWF weather analyses) the geometric mapping function displays above 6° elevation a comparable or better performance than other mapping functions currently in use.

An enhancement in the use of the geometric mapping function by introducing seasonal and geographical variations of the free parameter will further improve the performance, but already a global mean value works very well as demonstrated.

In a next step the new mapping function shall be tested with real data.

**Acknowledgements** The authors are indebted to S. Syndergaard (Univ. of Arizona, Tucson, AZ, U.S.A) for his very useful high-precision 3D ray tracer which needed only very modest modifications for the purpose of this work. We thank A. E. Niell (MIT, Boston, MA, U.S.A.) for providing valuable advice on the use of "mapping functions" and their limitations. The European Centre for Medium-Range Weather Forecasts (ECMWF) kindly provided the atmospheric analysis fields used. The work was financially supported by a START-Programm research award of the BM für Wissenschaft, Bildung und Kultur, under START research grant No. Y103-CHE of the Fonds zur Förderung der Wissenschaftlichen Forschung (FWF), Vienna, Austria.

## References

- Davis, J.L., Herring, T.A., Shapiro, I.I., Rogers, A.E.E., and Elgered, G., Geodesy by radio interferometry: Effects of atmospheric modeling errors on estimation of baseline length, *Radio Sci.*, 20, 1593-1607, 1985.
- Elgered, G., Tropospheric radio path delay from ground-based microwave radiometry, in *Atmospheric remote sensing by microwave radiometry*, edited by M.A. Janssen, Wiley & Sons, NY, 215-258, 1993.
- Marini, J.W., Correction of satellite tracking data for an arbitrary tropospheric profile, *Radio Sci.*, 7, 223-231, 1972.
- Niell, A.E., Global mapping functions for the atmosphere delay at radio wavelengths, *J. Geophys. Res.*, 101, 3227-3246, 1996.
- Saastamoinen, J., Introduction to practical computation of astronomical refraction, *Bulletin Géodésique*, 106, 383-397, 1972.